Supplementary Material

Large interdomain rearrangement triggered by suppression of micro- to millisecond dynamics in bacterial Enzyme I

Vincenzo Venditti,[1] Vitali Tugarinov,[1] Charles D. Schwieters,[2] Alexander Grishaev[1] and

G. Marius Clore[1,*]

[1]*Laboratory of Chemical Physics, National Institute of Diabetes and Digestive and Kidney Diseases, National Institutes of Health, Bethesda, Maryland 20892-0520, USA.*

[2]*Division of Computational Biosciences, Center for Information Technology, National Institutes of Health, Bethesda, Maryland 20892-0520, USA.*

*Correspondence and requests for materials should be addressed to G.M.C. (e-mail: mariusc@mail.nih.gov).

Supplementary Figures

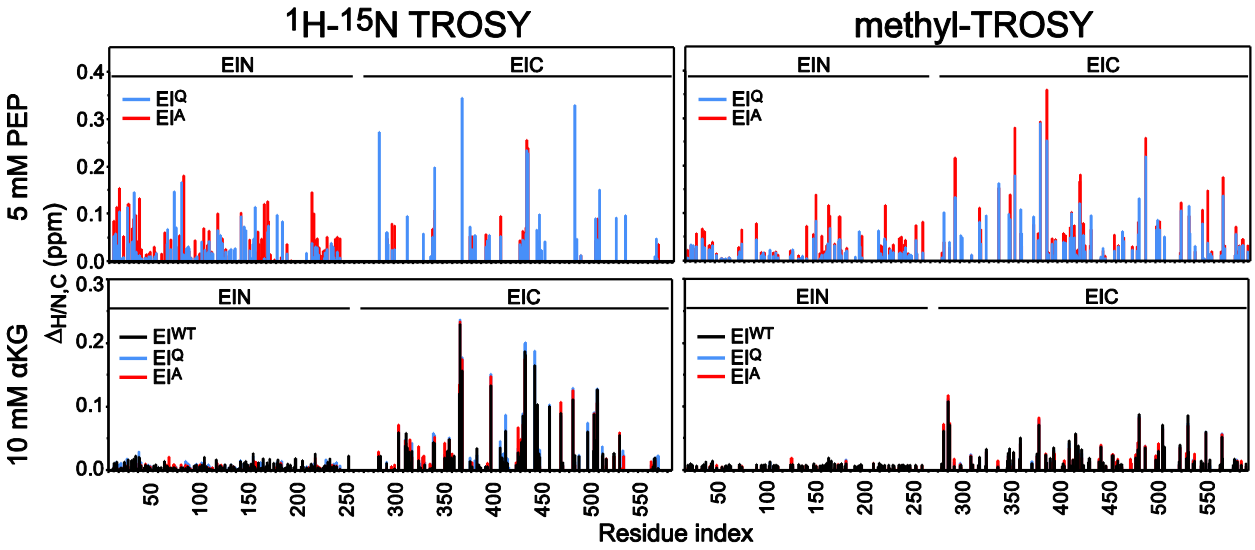

Figure 1. Effect of PEP and αKG on the NMR spectra of EI. Weighted combined chemical shift perturbations ($\Delta_{H/N,C}$) induced by PEP (top panel) and αKG (lower panel) on the ^1H_N-^{15}N (left panel) and ^1H-$^{13}C_{methyl}$ (right panel) TROSY correlation spectra of EI^{WT} (black), EI^Q (blue) and EI^A (red). Boundaries of the EIN and EIC domains in the full-length EI sequence are highlighted by black horizontal lines. αKG induces similar perturbations in all the analyzed samples. PEP generates larger $\Delta_{H/N,C}$ in the EI^A spectra, consistent with the larger population of closed EI detected by SAXS experiments on the EI^A-PEP complex (main text Fig. 3).

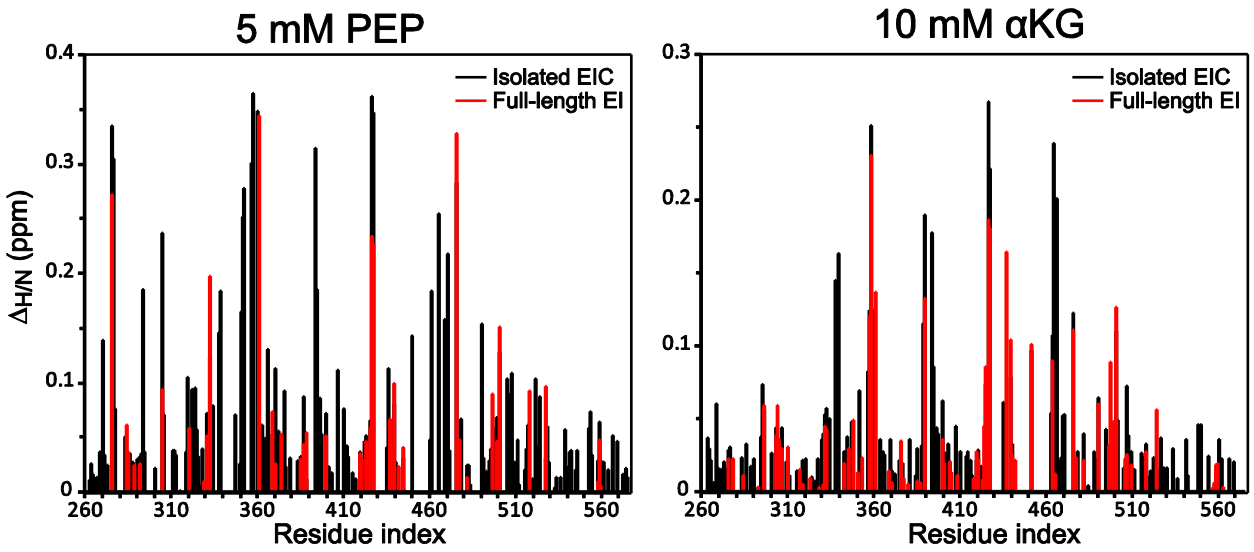

Figure 2. Comparison of the chemical shift perturbations in isolated EIC and full-length EI. Weighted combined chemical shift perturbations ($\Delta_{H/N}$) induced by PEP (left panel) and αKG (right panel) on the backbone amides of the EIC domain in the context of full-length EI (red) and the isolated EIC domain (black).

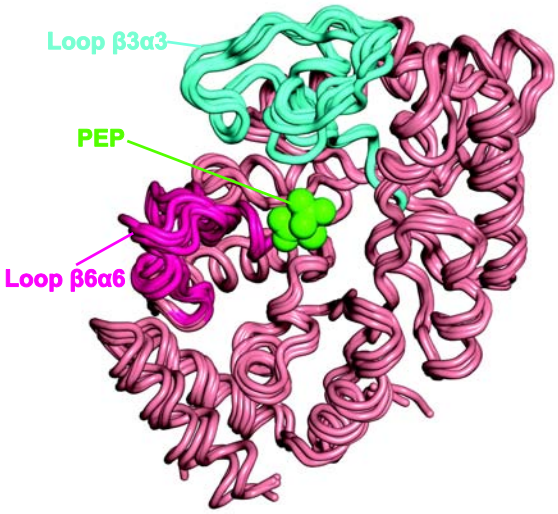

Figure 3. All the crystal structures of EI show similar EIC conformations. Overlay of all the X-ray structures solved to date for EIC (either in the isolated form or in the context of full-length EI). The following six structures are displayed: phosphorylated *E. coli* EI in complex with oxalate (pdb code: 2HWG),[1] EI from *Staphylococcus carnosus* (pdb code: 2HRO),[2] EI from *Staphylococcus aureus* (pdb code: 2WQD),[3] isolated EIC from *Thermoanaerobacter Tengcongensis* in the free form (pdb code: 2BG5)[4] and bound to PEP (pdb code: 2XZ7)[5] and pyruvate (pdb code: 2XZ9).[5] Only EIC domain residues are shown. The β3α3 (residues 333-366) and β6α6 (residues 453-477) loops are colored in cyan and purple, respectively. PEP is shown as green spheres. The average backbone r.m.s.d. between the structures and the mean coordinate positions calculated for residues 261-572 is 2.0 Å.

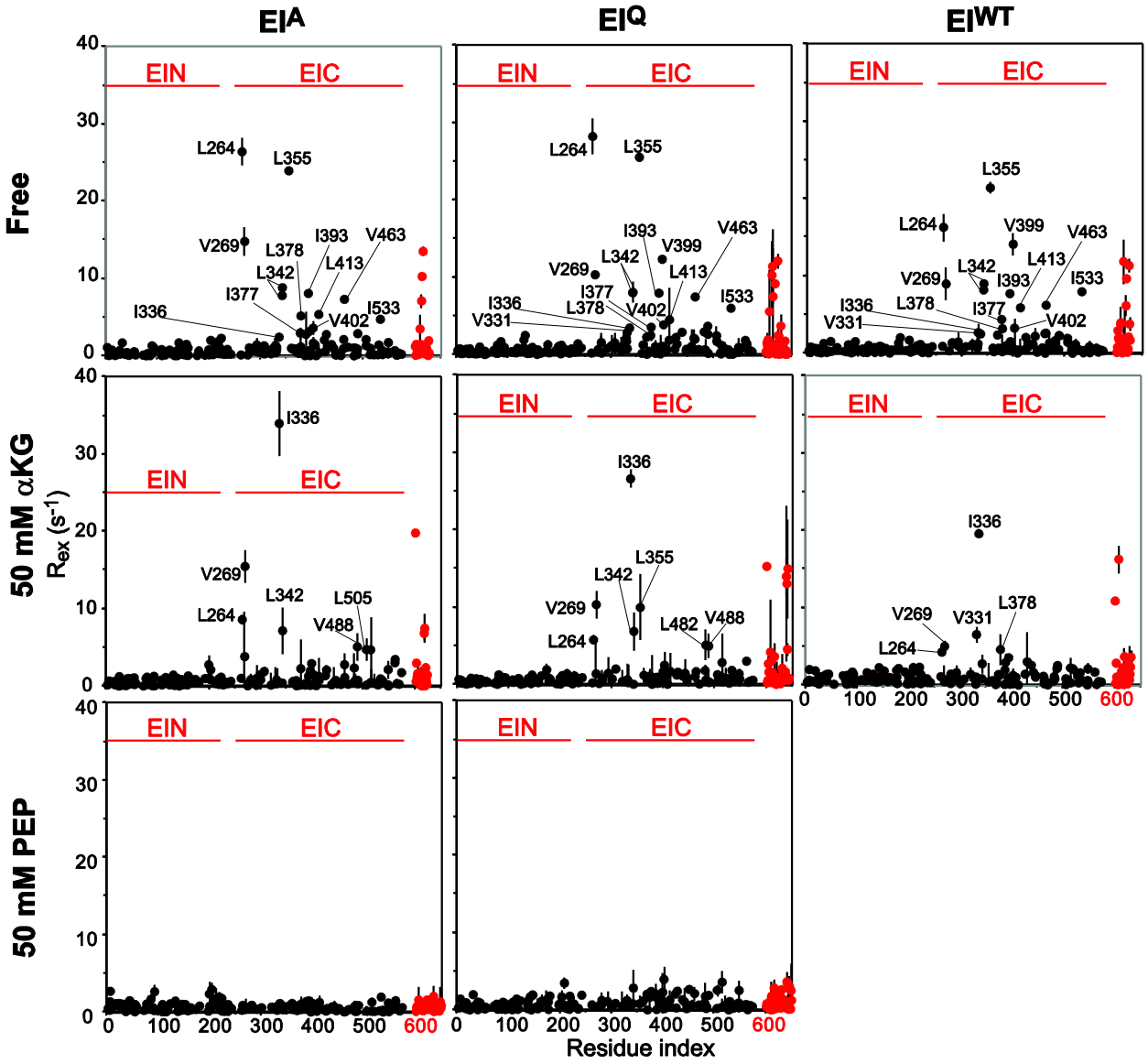

Figure 4. PEP suppresses µs-ms dynamics in the EIC domain of EI. Exchange contribution to the ^{1}H-$^{13}C_{methyl}$ transverse MQ-relaxation rates (MQ-R_{ex}) at 800 MHz measured for samples of EI^{A} (left panels), EI^{Q} (middle panels) and EI^{WT} (right panels) in the absence of ligands (top panels) and in the presence of 50 mM αKG (middle panels) and 50mM PEP (bottom panels). Data for unambiguously assigned cross-peaks are reported as black circles (residue index 1-575). Data for unassigned cross-peaks are shown as red circles (residue index > 600). Boundaries of the EIN and EIC domains in the full-length EI sequence are highlighted by red horizontal lines. Error bars: 1 s.d.

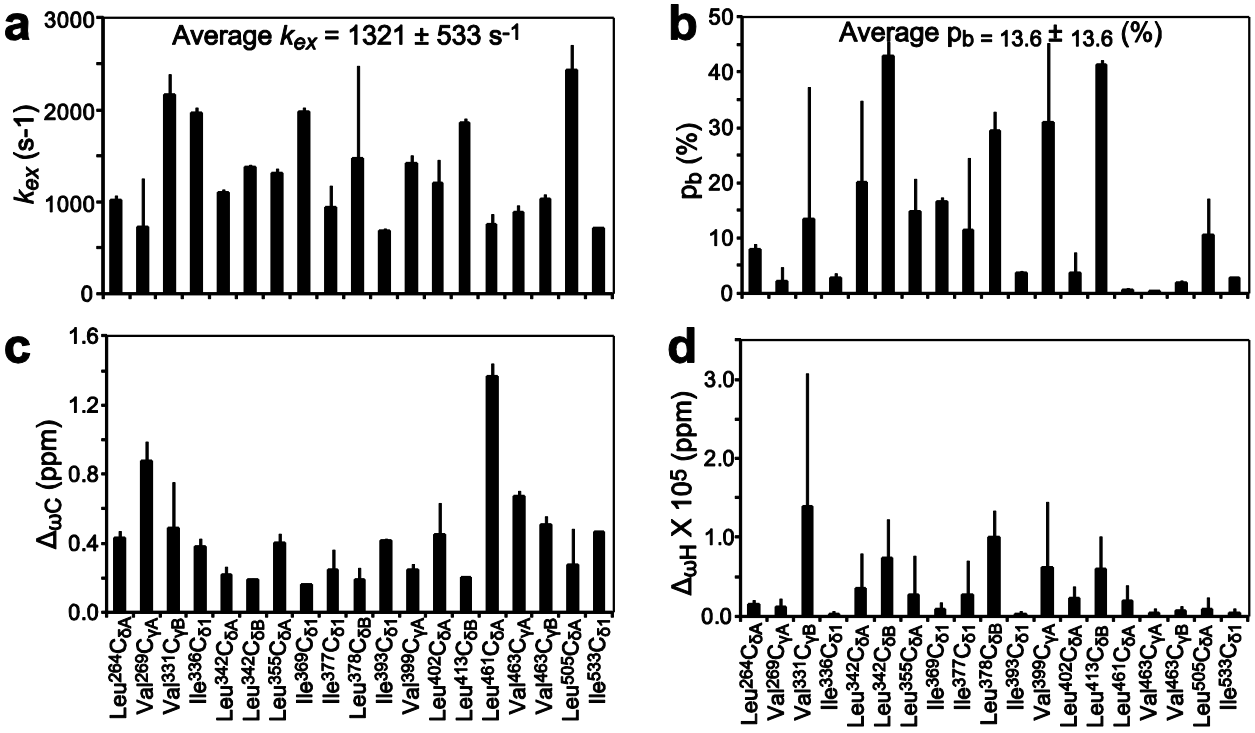

Figure 5. Residue-based fitting of the SQ and MQ relaxation dispersion data of free EI^{WT}. SQ and MQ relaxation dispersion curves acquired for 19 methyl groups of EIC in the context of free, full-length EI (see main text) were fitted using the Carver-Richards equations for a two-state exchange process (see Supporting Methods). In these plots the residue specific (**a**) k_{ex} , (**b**) p_b, (**c**) $\Delta\omega_C$ and (**d**) $\Delta\omega_H$ parameters resulting from the fitting procedure are reported. Error bars: 1 s.d.

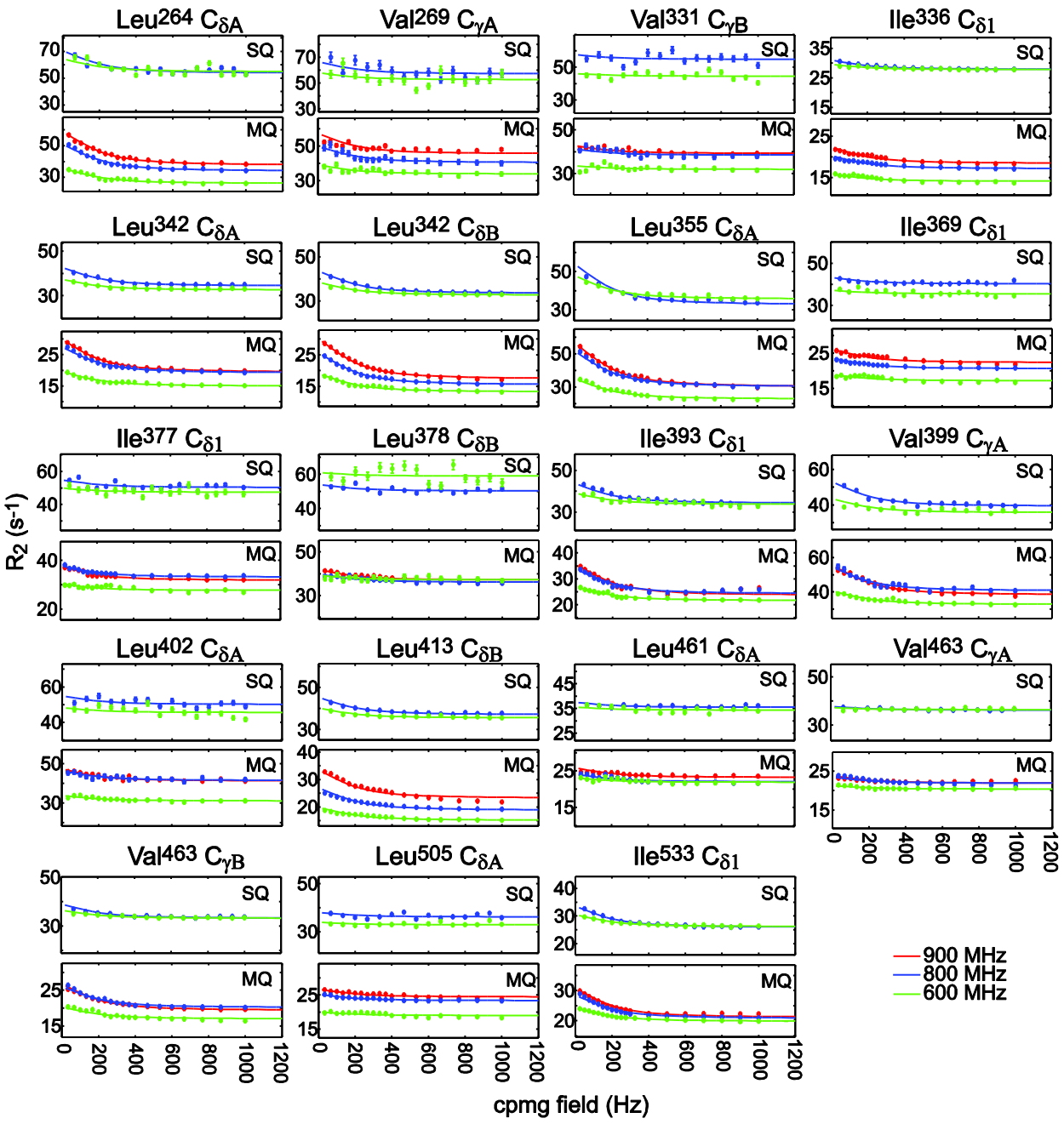

Figure 6. Global fitting of the SQ and MQ relaxation dispersion data of free EI^{WT}. SQ and MQ relaxation dispersion curves acquired for 19 methyl groups of EIC in the context of full length EI at 600 (green), 800 (blue) and 900 (red) MHz. Experimental data are reported as filled circles. Results of the global fit are shown as solid lines. Error bars: 1 s.d.

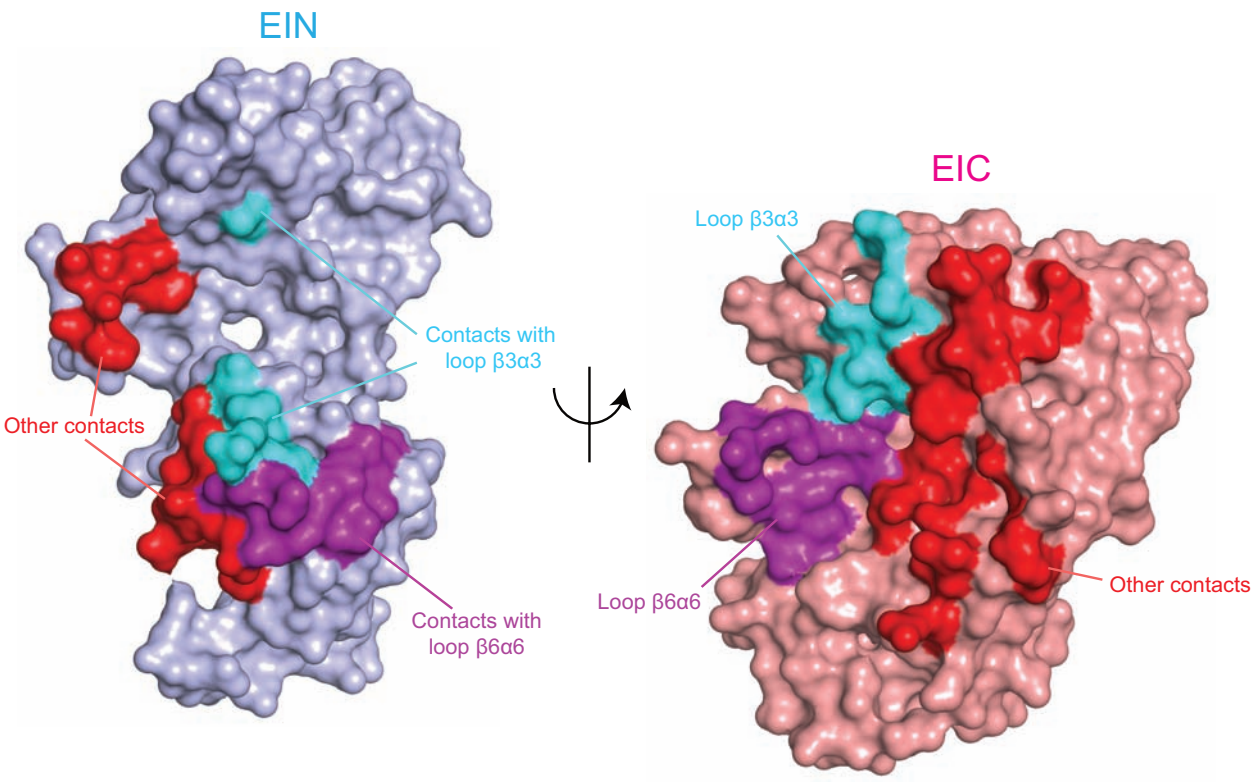

Figure 7. Interface between the EIN and EIC domains in the X-ray structure of the phosphorylated EI intermediate (closed state). The EIN (light blue, left) and EIC (pink, right) domains are shown as surfaces. Interdomain contacts involving the EIC loops β3α3 and β6α6 are colored cyan and purple, respectively. Other interdomain contacts are colored red.

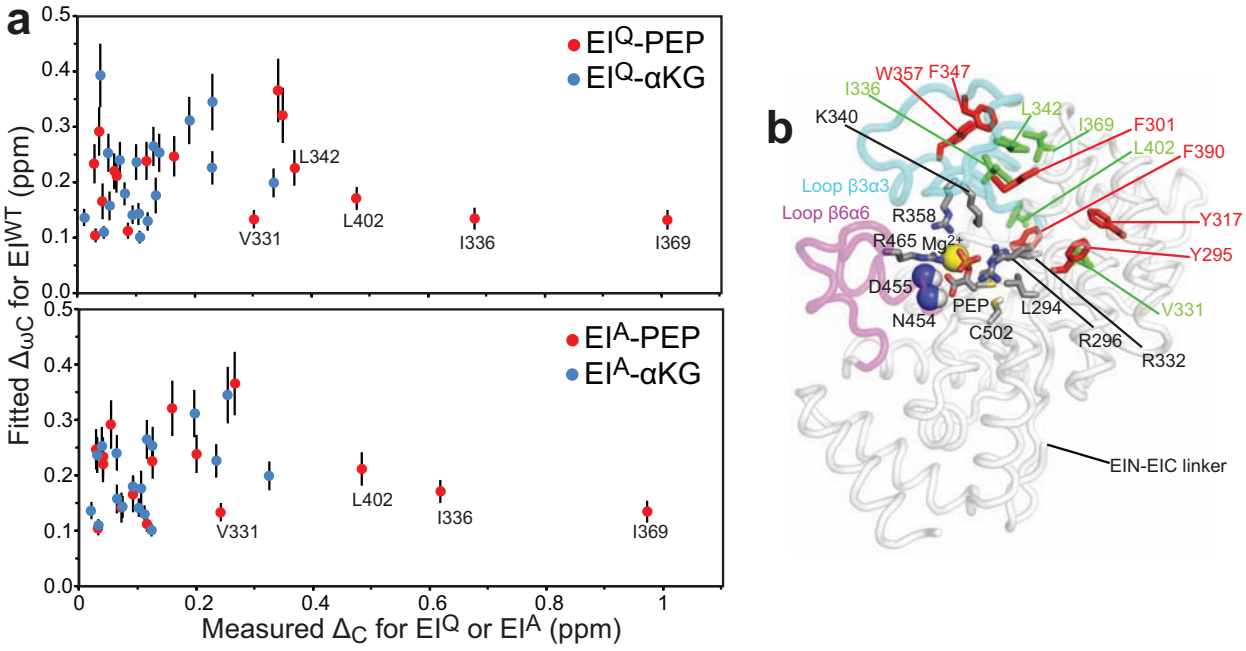

Figure 8. Comparison between $\Delta_{\omega C}$ and Δ_C values. (**a**) The $\Delta_{\omega C}$ parameters obtained from the fits to the relaxation dispersion data on EI^{WT} are plotted versus the Δ_C's induced by addition of 5 mM PEP (red circles) and 10 mM αKG (blue circles) to EI^Q (top) and EI^A (bottom) (**b**) Side chains for which $\Delta_C >> \Delta_{\omega C}$ are plotted as green sticks on the EIC structure. The β3α3 and β6α6 loops are colored cyan and purple, respectively. PEP and EIC side chains in the binding site are shown as sticks (carbon, gray; nitrogen, blue; oxygen, red; phosphorus, orange; sulfur, yellow). Mg^{2+} (yellow) and the amides of N454 and D455 (nitrogen, blue; hydrogen, white) are shown as spheres. The 5 side chains showing poor correlation between Δ_C and $\Delta_{\omega C}$ (V331, I336, L342, I369, and L402) are located in regions rich with aromatic residues (red sticks). Different packing of the aromatic side chains in the compact states sampled by EIC in the absence ($compact^I$) and presence ($compact^{II}$) of PEP may be responsible for the large deviations in the expected $\Delta_C/\Delta_{\omega C}$ correlation for the latter residues. Error bars: 1 s.d.

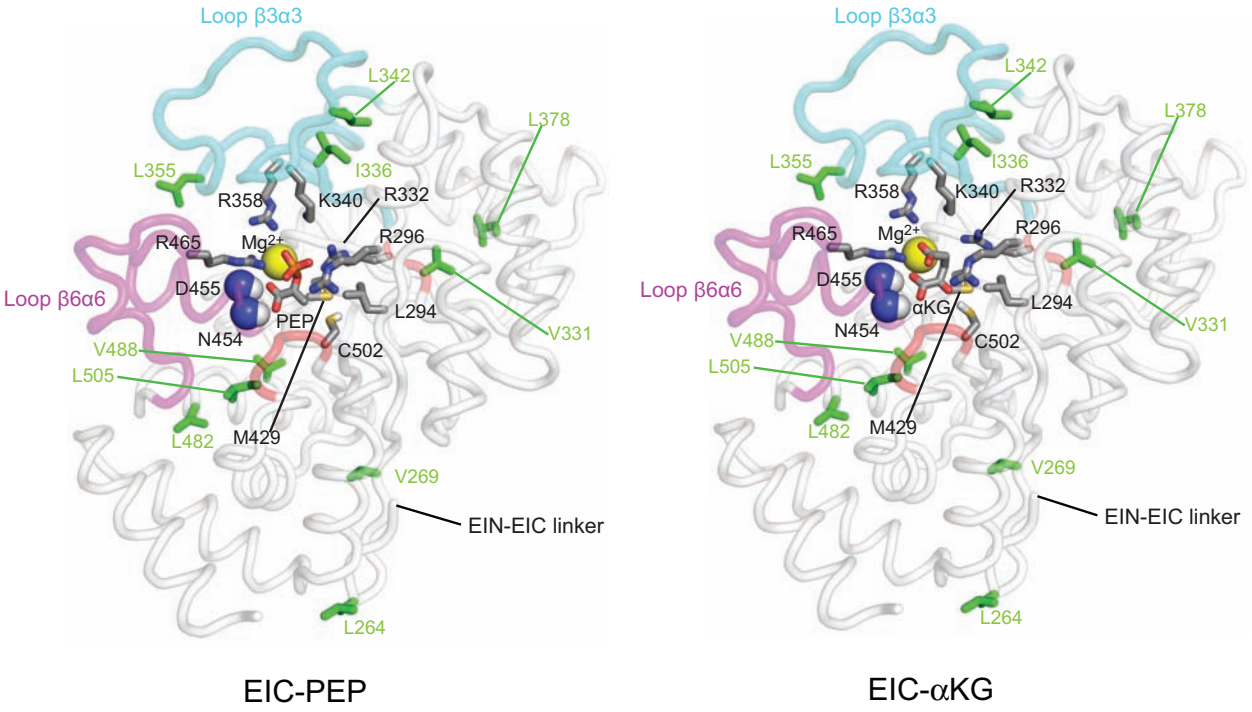

Figure 9. αKG reproduces only the interactions of PEP with the β6α6 loop. EIC complexes with PEP (left) and αKG (right). The β3α3 and β6α6 loops are colored cyan and purple, respectively. PEP, αKG and EIC side chains in the binding site are shown as sticks (carbon, gray; nitrogen, blue; oxygen, red; phosphorus, orange; sulfur, yellow). Mg^{2+} (yellow) and the amides (nitrogen, blue; hydrogen, white) of N454 and D455 are shown as spheres. Ile, Leu and Val side chains showing MQ-R_{ex} > 3 s^{-1} in the presence of 50 mM αKG are shown as green sticks. The portions of backbone connecting V331 and L505 to the binding site are colored red.

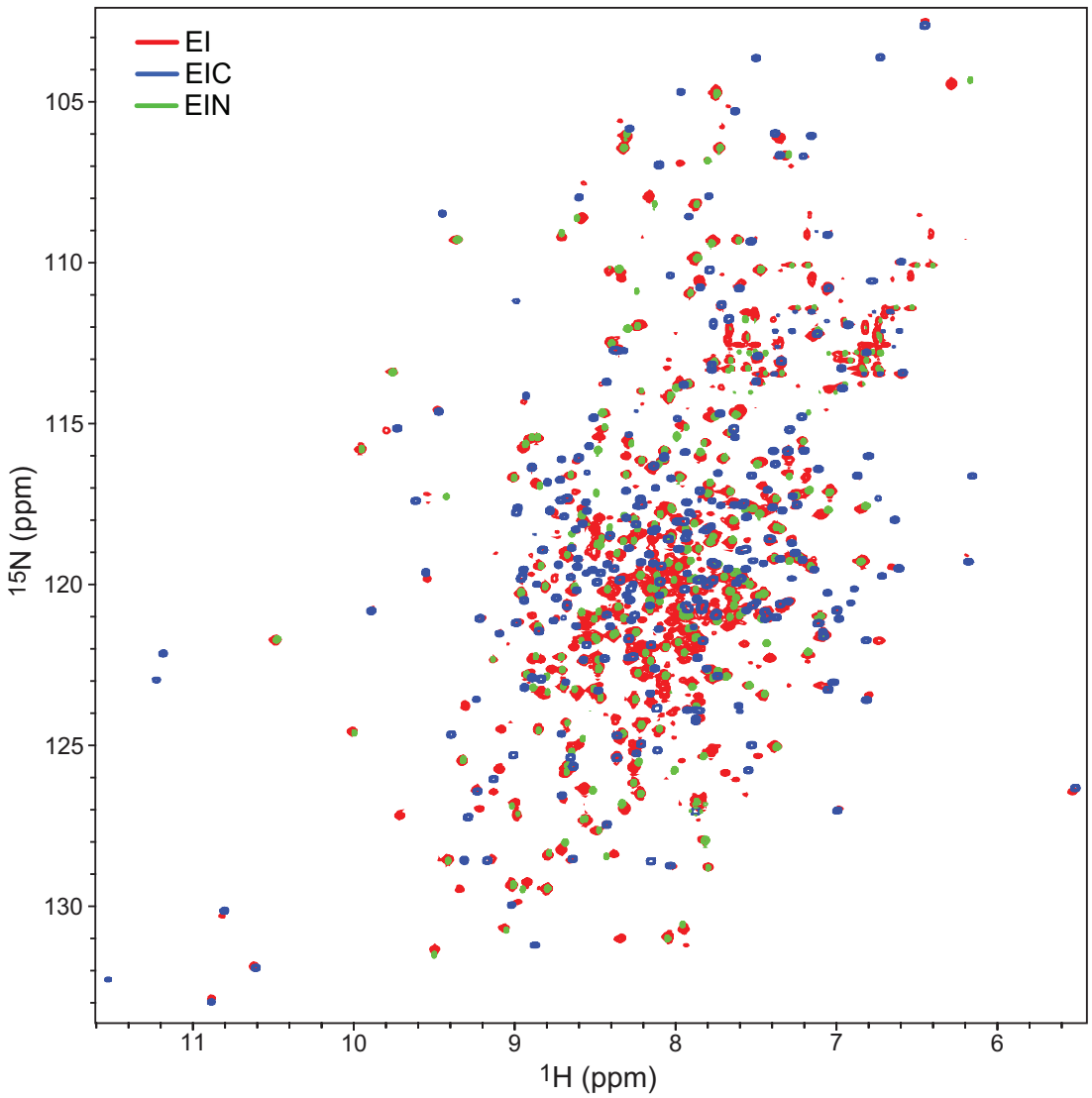

Figure 10. Assignment of the ^{1}H-^{15}N TROSY spectra of EI^{WT}. Overlay of the 900 MHz ^{1}H-^{15}N TROSY spectra of isolated EIN (green), isolated EIC (blue), and full-length EI (red), uniformly labeled with ^{15}N and non-exchangeable protons replaced by deuterium.

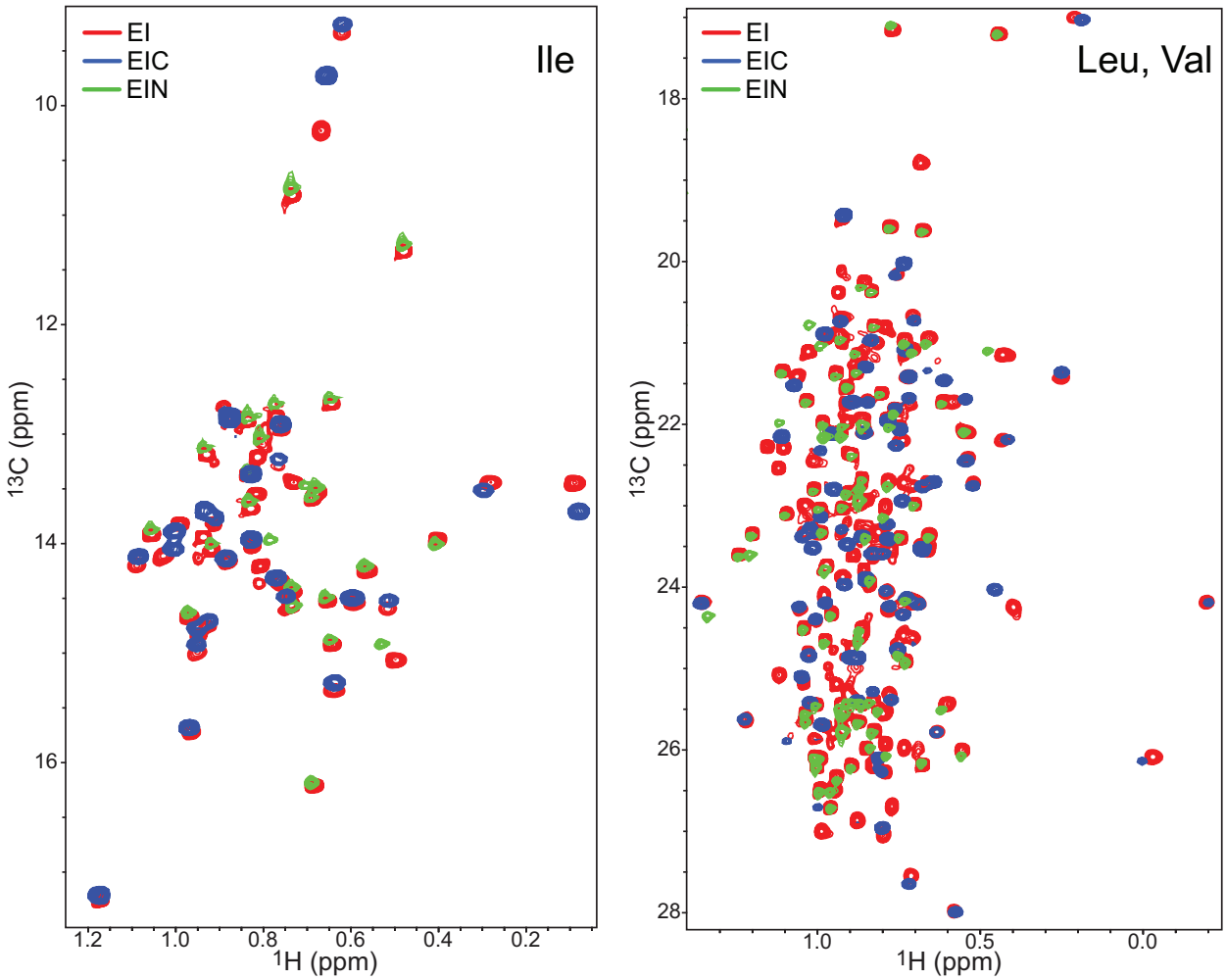

Figure 11. Assignment of the ^{1}H-$^{13}C_{methyl}$ TROSY spectra of EI^{WT}. Overlay of the 800 MHz ^{1}H-$^{13}C_{methyl}$ TROSY spectra of isolated EIN (green), isolated EIC (blue), and full-length EI (red) with either U-[^{2}H,^{15}N]/Ile(δ1)-$^{13}CH_3$ (left panel) and U-[^{2}H,^{15}N]/Val,Leu-($^{13}CH_3$/$^{12}C^{2}H_3$) (right panel) labeling.

Supplementary Table

Table 1. Methyl-specific ^{13}C chemical shift differences between major and minor states ($\Delta\omega_C$) obtained from the global fit of the MQ and SQ relaxation dispersion data on free EI.

Residue	$\Delta\omega_C$ (ppm)	Error (1 s.d.) (ppm)
L264-$C_{\delta A}$	0.35	0.05
V269-$C_{\gamma A}$	0.25	0.04
V331-$C_{\gamma B}$	0.14	0.02
I336-$C_{\delta 1}$	0.15	0.02
L342-$C_{\delta A}$	0.24	0.03
L342-$C_{\delta B}$	0.27	0.04
L355-$C_{\delta A}$	0.40	0.06
I369-$C_{\delta 1}$	0.14	0.02
I377-$C_{\delta 1}$	0.18	0.03
L378-$C_{\delta B}$	0.16	0.03
I393-$C_{\delta 1}$	0.26	0.03
V399-$C_{\gamma A}$	0.31	0.04
L402-$C_{\delta A}$	0.18	0.02
L413-$C_{\delta B}$	0.24	0.03
L461-$C_{\delta A}$	0.12	0.01
V463-$C_{\gamma A}$	0.10	0.01
V463-$C_{\gamma B}$	0.20	0.03
L505-$C_{\delta A}$	0.11	0.01
I533-$C_{\delta 1}$	0.23	0.03

Supplementary Methods

Fitting of the MQ and SQ CPMG ^{13}C-relaxation dispersion curves

The ^{1}H-^{13}C MQ and ^{13}C SQ CPMG relaxation dispersion curves were best fit to analytical expressions for the effective MQ and SQ R_2 of the EI resonances as a function of the CPMG field (1/4δ), valid in all exchange and population regimes:[6, 7]

-MQ fit

$$R_{2,eff}^{MQ}\left(\frac{1}{2\delta}\right) = \mathrm{Re}\left(\lambda_1\right) - \frac{1}{4n\delta}\ln\left(Q\right) \tag{1}$$

with

$$\lambda_1 = R_2^{MQ} + \frac{1}{2}\left(k_{ex} - \frac{1}{2\delta}\cosh^{-1}\left(D_+\cosh\eta_+ - D_-\cos\eta_-\right)\right) \tag{2}$$

$$D_\pm = \frac{1}{2}\left(\frac{\Psi + 2\Delta\omega_C^2}{\sqrt{\Psi^2 + \zeta^2}} \pm 1\right) \tag{3}$$

$$\eta_\pm = \sqrt{2}\delta\sqrt{\sqrt{\Psi^2 + \zeta^2} \pm \Psi} \tag{4}$$

$$\Psi = \left(i\Delta\omega_H + \left(p_a - p_b\right)k_{ex}\right)^2 - \Delta\omega_C^2 + 4p_a p_b k_{ex}^2 \tag{5}$$

$$\zeta = -2\Delta\omega_C\left(i\Delta\omega_H + \left(p_a - p_b\right)k_{ex}\right) \tag{6}$$

$$Q = \mathrm{Re}\left(1 - m_D^2 + m_D m_Z - m_Z^2 + (1/2)(m_D + m_Z)\sqrt{p_b/p_a}\right) \tag{7}$$

$$m_D = \frac{ik_{ex}\sqrt{p_a p_b}}{d_+ z_+}\left(z_+ + 2\Delta\omega_C \frac{\sin(z_+\delta)}{\sin((d_+ + z_+)\delta)}\right) \tag{8}$$

$$m_Z = \frac{ik_{ex}\sqrt{p_a p_b}}{d_- z_-}\left(z_- + 2\Delta\omega_C \frac{\sin(d_-\delta)}{\sin((d_- + z_-)\delta)}\right) \tag{9}$$

$$d_\pm = (\Delta\omega_H + \Delta\omega_C) \pm ik_{ex},\ z_\pm = (\Delta\omega_H - \Delta\omega_C) \pm ik_{ex} \tag{10}$$

-SQ fit

$$R_{2,eff}^{SQ}\left(\frac{1}{2\delta}\right) = \mathrm{Re}(\lambda_1) - \frac{1}{4n\delta}\ln(Q) \tag{11}$$

with

$$\lambda_1 = R_2^{SQ} + \frac{1}{2}\left(k_{ex} - \frac{1}{2\delta}\cosh^{-1}(D_+\cosh\eta_+ - D_-\cos\eta_-)\right) \tag{12}$$

$$D_\pm = \frac{1}{2}\left(\frac{\Psi + 2\Delta\omega_C^2}{\sqrt{\Psi^2 + \zeta^2}} \pm 1\right) \tag{13}$$

$$\eta_\pm = \sqrt{2}\delta\sqrt{\sqrt{\Psi^2 + \zeta^2} \pm \Psi} \tag{14}$$

$$\Psi = ((p_a - p_b)k_{ex})^2 - \Delta\omega_C^2 + 4p_a p_b k_{ex}^2 \tag{15}$$

$$\zeta = -2\Delta\omega_C((p_a - p_b)k_{ex}) \tag{16}$$

$$Q = \mathrm{Re}\left(1 - m_D^2 + m_D m_Z - m_Z^2 + (1/2)(m_D + m_Z)\sqrt{p_b/p_a}\right) \tag{17}$$

$$m_D = \frac{ik_{ex}\sqrt{p_a p_b}}{d_+ z_+}\left(z_+ + 2\Delta\omega_C \frac{\sin(z_+\delta)}{\sin((d_+ + z_+)\delta)}\right) \quad (18)$$

$$m_Z = \frac{ik_{ex}\sqrt{p_a p_b}}{d_- z_-}\left(z_- + 2\Delta\omega_C \frac{\sin(d_-\delta)}{\sin((d_- + z_-)\delta)}\right) \quad (19)$$

$$d_\pm = \Delta\omega_C \pm ik_{ex},\ z_\pm = -\Delta\omega_C \pm ik_{ex} \quad (20)$$

Here, R_2^{MQ} and R_2^{SQ} are the multiple and single quantum transverse relaxation rates, respectively; n is the number of 180° refocusing pulses in the CPMG train; 2δ is the spacing between the centers of successive 180° pulses; k_{ex} is the exchange rate constant; p_a and p_b are the fractional populations of the major and minor species, respectively; $\Delta\omega_C$ and $\Delta\omega_H$ (rad s^{-1}) are the carbon and proton chemical shift differences between the two conformational states, respectively.

Fitting of SAXS data

The calcSAXS-bufSub helper program uses an adaptation of the AXES algorithm[8] in which sample background subtraction is performed during the fit procedure, such that one must provide scattering curves for both the sample and for the buffer solution. The experimental curve to fit against is given by

$$I_{\text{expt}}(q) = I_{\text{sample}}(q) - \alpha I_{\text{buffer}}(q) + c \quad (21)$$

where α is a scale factor taking values near one and c is a constant background value. The scattering factor q is related to the experimental scattering angle 2θ by

$$q = 4\pi\sin(\theta)/\lambda \quad (22)$$

where λ is the wavelength of the incident radiation. A description of the motivation for the choice of the form of Eq. (21) is given in ref. 8.

The scattering curve calculated from a molecular structure is given by

$$I_{\mathrm{calc}}(q) = N\langle|\mathrm{A}(\mathbf{q}) + p_b A_b(\mathbf{q})|^2\rangle_\Omega \qquad (23)$$

where N is an overall normalization, $A(\mathbf{q})$ is the scattering amplitude due to the molecular structure minus the contribution of occluded solvent at position $\mathbf{q}$ in reciprocal space, and $A_\mathrm{b}(\mathbf{q})$ is the scattering amplitude contribution from surface-bound solvent with effective density p_B. $A(\mathbf{q})$ and $A_\mathrm{b}(\mathbf{q})$ correspond to the two terms in Eq. (21) of ref. 9 and are computed as described there. $\langle\cdot\rangle_\Omega$ denotes average over solid angle.

As in ref. 8, α, c, N and p_b are determined using gradient-based minimization of a cost function comprised of the sum of the SAXS χ^2 and a small regularization term. The calcSAXS-bufSub helper program can calculate the weighted average SAXS curves over multiple structures required in this work. It is distributed with Xplor-NIH starting with version 2.37.

Supplementary References

1. Teplyakov A*, et al.* Structure of phosphorylated enzyme I, the phosphoenolpyruvate:sugar phosphotransferase system sugar translocation signal protein. *Proc Natl Acad Sci U S A* **103**, 16218-16223 (2006).
2. Marquez J, Reinelt S, Koch B, Engelmann R, Hengstenberg W, Scheffzek K. Structure of the full-length enzyme I of the phosphoenolpyruvate-dependent sugar phosphotransferase system. *J Biol Chem* **281**, 32508-32515 (2006).
3. Oberholzer AE, Schneider P, Siebold C, Baumann U, Erni B. Crystal structure of enzyme I of the phosphoenolpyruvate sugar phosphotransferase system in the dephosphorylated state. *J Biol Chem* **284**, 33169-33176 (2009).
4. Oberholzer AE*, et al.* Crystal structure of the phosphoenolpyruvate-binding enzyme I-domain from the *Thermoanaerobacter tengcongensis* PEP:sugar phosphotransferase system (PTS). *J Mol Biol* **346**, 521-532 (2005).
5. Navdaeva V*, et al.* Phosphoenolpyruvate: sugar phosphotransferase system from the hyperthermophilic *Thermoanaerobacter tengcongensis*. *Biochemistry* **50**, 1184-1193 (2011).
6. Carver JP, Richards RE. A general two-site solution for the chemical exchange produced dependence of T_2 upon the Carr-Purcell pulse separation. *J Magn Reson* **6**, 89-105 (1972).

7. Korzhnev DM, Kloiber K, Kanelis V, Tugarinov V, Kay LE. Probing slow dynamics in high molecular weight proteins by methyl-TROSY NMR spectroscopy: application to a 723-residue enzyme. *J Am Chem Soc* **126**, 3964-3973 (2004).
8. Grishaev A, Guo L, Irving T, Bax A. Improved fitting of solution X-ray scattering data to macromolecular structures and structural ensembles by explicit water modeling. *J Am Chem Soc* **132**, 15484-15486 (2010).
9. Schwieters CD, Clore GM. Using small angle solution scattering data in Xplor-NIH structure calculations. *Prog Nucl Magn Reson Spectrosc* **80**, 1-11 (2014).